JACS
JOURNAL OF THE AMERICAN CHEMICAL SOCIETY

Article

pubs.acs.org/JACS

Circumventing Diffusion in Kinetically Controlled Solid-State Metathesis Reactions

Andrew J. Martinolich, Joshua A. Kurzman, and James R. Neilson*

Department of Chemistry, Colorado State University, Fort Collins, Colorado 80523-1872, United States

Supporting Information

ABSTRACT: Solid-state diffusion is often the primary limitation in the synthesis of crystalline inorganic materials and prevents the potential discovery and isolation of new materials that may not be the most stable with respect to the reaction conditions. Synthetic approaches that circumvent diffusion *in solid-state reactions* are rare and often allow the formation of metastable products. To this end, we present an *in situ* study of the solid-state metathesis reactions MCl_2 + Na_2S_2 → MS_2 + 2 NaCl (M = Fe, Co, Ni) using synchrotron powder X-ray diffraction and differential scanning calorimetry. Depending on the preparation method of the reaction, either combining the reactants in an air-free environment or grinding homogeneously in air before annealing, the barrier to product formation, and therefore reaction pathway, can be altered. In the air-free reactions, the product formation appears to be diffusion limited, with a number of intermediate phases observed before formation of the MS_2 product. However, grinding the reactants in air allows NaCl to form directly without annealing and displaces the corresponding metal and sulfide ions into an amorphous matrix, as confirmed by pair distribution function analysis. Heating this mixture yields direct nucleation of the MS_2 phase and avoids all crystalline binary intermediates. Grinding in air also dissipates a large amount of lattice energy via the formation of NaCl, and the crystallization of the metal sulfide is a much less exothermic process. This approach has the potential to allow formation of a range of binary, ternary, or higher-ordered compounds to be synthesized in the bulk, while avoiding the formation of many binary intermediates that may otherwise form in a diffusion-limited reaction.

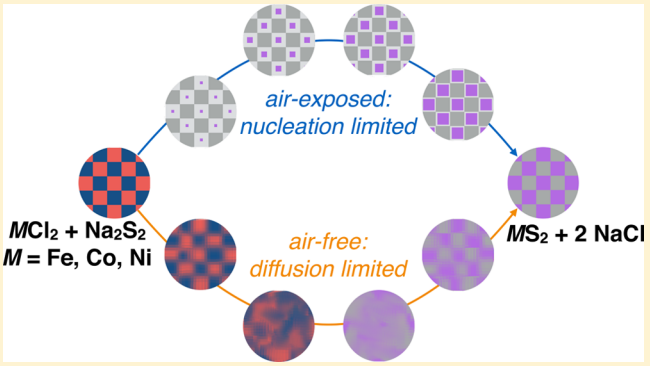

INTRODUCTION

Solid-state chemical reactions are impeded by diffusion. Therefore, comparatively little can be done to gain kinetic control of solid-state chemical reactions in contrast to other fields of synthetic chemistry.[1−3] Instead, much reliance is put into reaching conditions in which solid-state diffusion is enhanced (i.e., higher temperatures) and the reactants are allowed to equilibrate and form the products that are most stable in that environment. Syntheses of nanomaterials are now approaching a "total-synthesis" framework to rationally design and tailor colloidal assemblies.[4]

Generally, the formation of metastable solid materials relies on chemical (de)intercalation or exchange of one type of ion from the lattice while the other ions remain immobilized in the lattice. This can be achieved in solution[5−7] or in the solid phase[8−10] to form metastable materials that are structurally analogous to the stable precursor but with a different composition. This inherently limits these processes to materials with mobile ions and a framework that can be oxidized or reduced and maintain its structure. Reactive alkali chalcogenide fluxes have the ability to enhance diffusion at moderate temperatures,[11] but the predictability of these reactions is in its infancy.[12,13] Solid-state metathesis (i.e., double ion exchange) reactions permit compositional predictability and allow for the initiation of solid-state reactions at low temperatures due to the formation of a thermodynamically stable byproduct, such as NaCl. These reactions initially garnered excitement for their ability to self-ignite to achieve short-lived temperatures in excess of 1000 °C, thus permitting the preparation of refractory[14−20] and ultrahard materials.[21−23] More recently, our group has shown that, with nonigniting reactions, solid-state metathesis can be performed in the limit of kinetic control,[24] and the reaction pathway can be chemically altered in order to isolate metastable phases.[25,26]

Here, we study solid-state metathesis reactions, MCl_2 + Na_2S_2 (M = Fe, Co, Ni), prepared in two different ways so as to proceed in either a diffusion-limited or a nucleation-limited manner. The reaction MCl_2 + Na_2S_2 (M = Fe, Co, Ni) prepared in strictly inert conditions reacts through a diffusion-limited pathway, forming several substoichiometric M_xS_y ($2x > y$) intermediates before the stoichiometric MS_2 product, as determined by *in situ* synchrotron powder X-ray diffraction. Correlation of these *in situ* diffraction data to differential scanning calorimetry (DSC) indicates that the NaCl formation is slow and only mildly exothermic in the strictly anhydrous

Received: June 20, 2016
Published: August 4, 2016

DOI: 10.1021/jacs.6b06367
J. Am. Chem. Soc. 2016, 138, 11031−11037

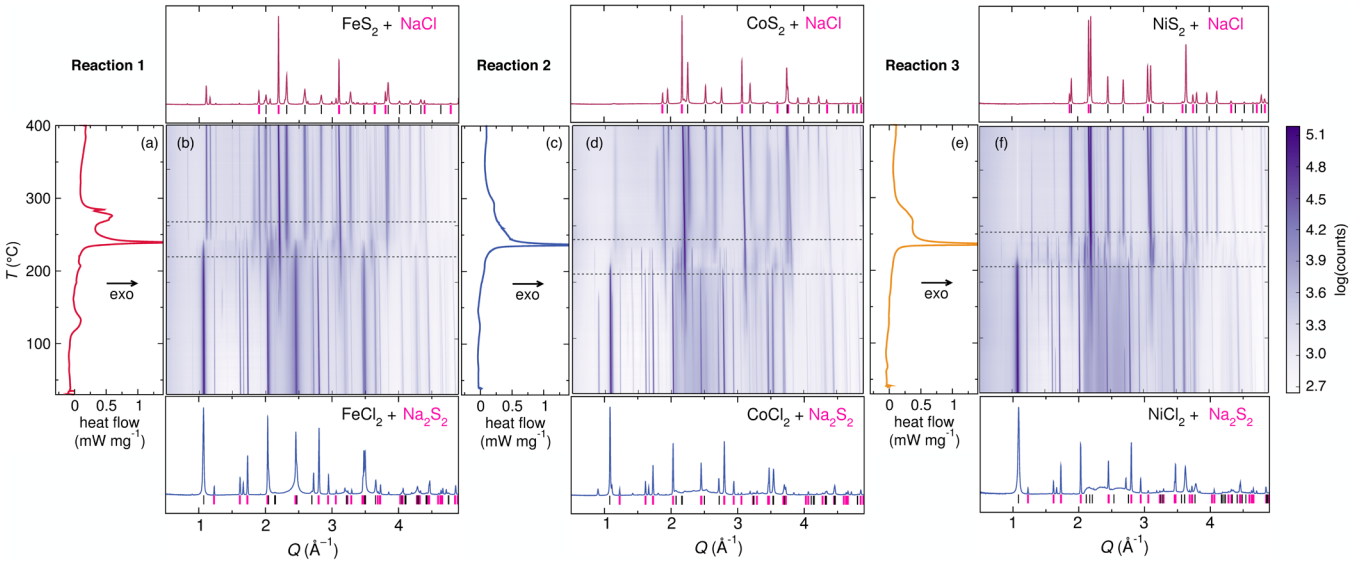

Figure 1. *In situ* DSC (a, c, e) and SXRD (b, d, f) of the strictly anhydrous solid-state metathesis reactions of $MCl_2 + Na_2S_2 \rightarrow MS_2 + 2$ NaCl, where M = Fe (reaction **1**), Co (reaction **2**), and Ni (reaction **3**), respectively. Each reaction progresses through three major zones: reactants at low temperatures (bottom panels), a highly reactive zone with transient intermediates with the major exotherm in the DSC (between dashed lines), and the expected products at high temperatures (top panels). Color plots are shown on a logarithmic scale to accentuate minor phase contributions during the reactive zone.

Table 1. Summary of Product Formation Temperatures, Intermediates, and Energetics in Reactions 1−6

reaction	reactive zone T	T_f (MS_2)	T_f (NaCl)	crystalline intermediates	integrated exotherm (kJ mol^{-1})	theoretical reaction enthalpy (kJ mol^{-1})
1	222−257 °C	222 °C	115 °C	Na_2S_4, Na_2S_5, Fe_7S_8, Fe_3S_4, $Na_3Fe_2S_4$, marcasite FeS_2	−141	−261
2	192−230 °C	260 °C	100 °C	Na_2S_4, Na_2S_5, Co_9S_8, CoS, Co_3S_4	−133	−263
3	196−242 °C	228 °C	90 °C	Na_2S_4, Ni_3S_2, ht-NiS, rt-NiS	−137	−249
4	n/a	155 °C	n/a	none	−15	−261
5	n/a	240 °C	n/a	none	−13	−263
6	n/a	155 °C	n/a	none	−36	−249

reactions, in contrast to the standing hypothesis that these reactions are driven by the formation of the NaCl byproducts. However, if the reactants are first exposed to humid air, NaCl formation occurs immediately upon grinding at room temperature, thus displacing the counterions into an amorphous matrix resembling known M−S phases with low coordination numbers. Heating this mixture nucleates the crystalline MS_2 phase directly without substoichiometric intermediates. In these partially hydrated reactions, the DSC does not show significant enthalpic signatures upon crystallization of the product. Together, our results provide an approach to overcome solid-state diffusion in a bulk solid-state reaction and provide insight into the mechanistic control of solid-state reactions.

RESULTS

The reactions $MCl_2 + Na_2S_2 \rightarrow 2NaCl + MS_2$ (M = Fe, Co, or Ni) have been previously reported, and the reactions typically require heating the reactants to $T \geq 250$ °C for the reaction to proceed when performed in anhydrous conditions.[20,24] In this contribution, these reactions are described in detail from experiments involving *in situ* synchrotron X-ray diffraction (SXRD, under vacuum) and differential scanning calorimetry (DSC, under argon) to study their reaction progress and energetic profiles as a function of temperature from the range 25 °C $\leq T \leq$ 400 °C. The reactions were performed two different ways and will be discussed in the following order: (a) the reactants were initially ground in an Ar-filled glovebox, and then heated in vacuum (SXRD) or argon (DSC); (b) the reactants were initially ground in air, and then heated in vacuum (SXRD) or argon (DSC).

The anhydrous reactions $MCl_2 + Na_2S_2 \rightarrow MS_2 + 2$ NaCl (M = Fe, reaction **1**; Co, reaction **2**; Ni, reaction **3**), mixed under argon and prepared for analysis without exposure to air, were studied upon heating within the range 25 °C $\leq T \leq$ 400 °C using DSC (Figure 1a,c,e) and SXRD (Figure 1b,d,f). Each reaction occurs in a similar fashion, progressing from reactants to products with the exothermic formation of multiple crystalline intermediates. A detailed description of each reaction is provided in the Supporting Information, and a summary of the observed crystalline intermediates is provided in Table 1.

As the reactants are heated, the first phase to crystallize in appreciable amounts is NaCl. This occurs at relatively low temperatures ($T \approx 100$ °C) in **1**−**3**. In all cases, various sodium sulfide intermediates also crystallize concomitant with NaCl formation. A small exotherm is also observed in **1** at $T \approx 130$ °C that may be attributed to the formation of NaCl; an obvious exotherm is not visible in **2** or **3** with the initial formation of NaCl. The small exotherm may also be attributed to the slow, gradual formation of NaCl which spreads out the release of heat over a large range of temperatures. Along with NaCl formation is the appearance of several sodium-poor Na−S phases (e.g., Na_2S_4 and Na_2S_5). The appearance of sulfur-poor binary M−S

DOI: 10.1021/jacs.6b06367
J. Am. Chem. Soc. 2016, 138, 11031−11037

phases (e.g., Fe_7S_8, Fe_3S_4, Co_9S_8, CoS, Co_3S_4, Ni_3S_2, and NiS), and one ternary $Na_3Fe_2S_4$ phase, occurs approximately at the temperature of the major exotherm. Several of these intermediate phases are expected to be metastable under the experimental conditions according to their bulk equilibrium phase diagrams,[27−29] such as spinel Fe_3S_4, marcasite FeS_2, hexagonal CoS, and the high-temperature polymorph of NiS. Representative Rietveld analyses of diffraction patterns taken during this intermediate reactive period are shown in Figure S1. The end of the reactive zone concludes with formation of the expected MS_2 phase. Integration of the DSC curves (correcting for a linear sloping baseline offset) yields the integrated reaction enthalpy, which is lower than the theoretical reaction enthalpy determined from Hess's Law (Table 1), in contrast to the self-igniting metathesis reactions.[15,17] Comparison of the temperature of the major exotherm detected via DSC to the relative phase fractions of the reactants and products indicates that *the sharp exotherm is not due to the formation of NaCl*, but instead due to reactivity of the metal sulfide phases and MS_2 product formation (Figure 2).

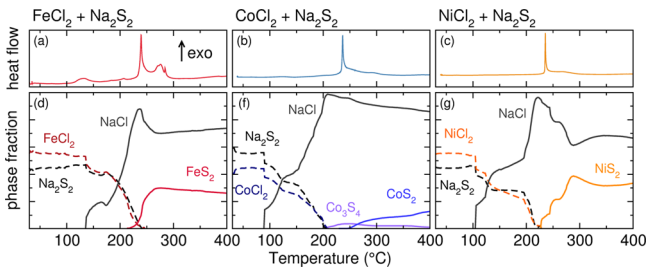

Figure 2. DSC (a−c) compared to relative crystalline phase fractions (d−f) of the reactants and the majority products as a function of temperature extracted from sequential Rietveld refinements indicating the general reaction progression of the air-free solid-state metathesis reactions (omitting other crystalline intermediates with <10 mol % phase fractions). The phase fraction of NaCl peaks before the major exotherm, indicating that the exotherm is released due to the crystallization and progression of the MS_x phases.

The reactions follow a completely different pathway if the reactants are exposed to air before preparation for DSC and *in situ* SXRD (M = Fe, reaction **4**; Co, reaction **5**; Ni, reaction **6**; Figure 3a−f). In all cases, crystalline NaCl forms upon grinding the reactants in air at room temperature. The yield of NaCl immediately after grinding is approximately 50 mol% of the expected in all cases, determined via PXRD with a known amount of internal Si standard. There is a significant amount of diffuse scattering visible in the diffraction data after subtraction of the silica capillary background. There is also a small amount of $NaFeS_2$ and elemental sulfur detected at room temperature in **4**, similar to our previous *ex situ* study.[24]

As the reaction mixture is heated, the expected MS_2 product crystallizes directly, and the diffuse background decreases. In contrast to the air-free experiments, there is no apparent reactive zone, no progression of crystalline M−S binary intermediates, and no polymorphism in the products. The distinct DSC results show subtle endothermic processes at low temperatures with a small exotherm observed upon MS_2 crystallization. Integration of the exotherms indicates that these processes are an order of magnitude less exothermic than the air-free reactions. At 400 °C, the ratio of NaCl to MS_2 is approximately 2:1 in all cases as anticipated from the balanced chemical reaction. These results, along with those from reactions **1**−**3**, are summarized in Table 1.

To probe the nature of the diffuse scattering in the air-exposed reactions, the structure of the residual metal sulfide was investigated using pair distribution function (PDF) analysis of total X-ray scattering data of the as-ground mixture (Figure 4) and as a function of temperature for reaction **4** (Figure 5 and Figure S6). In the as-ground samples, a majority of the correlations visible in the PDF correspond to highly crystalline NaCl, as quantitatively modeled. Therefore, after constraining the NaCl phase to fit the PDF at longer r (r > 10 Å), the difference between the NaCl fit and the experimental PDF reveals the short-range order of an amorphous metal sulfide phase with a low coordination number. Comparison of this difference curve to calculated PDFs of various spherically truncated crystalline metal sulfides indicates that the phases have short-range order that is structurally similar, but not the same, as that of intermediate MS phases or the resultant MS_2 products that form. The nearest-neighbor pair correlation peak appears at a distance consistent with known M−S phases, rather than M−O or M−Cl bond lengths as indicated in Figure 4. Low r correlations in the *in situ* PDF analysis of reaction **4** (Figure 5) also indicates that a short range ordered intermediate forms upon air exposure. The amorphous intermediate resembles a combination of pyrite FeS_2 and tetragonal FeS. This then crystallizes to pyrite FeS_2 at T ≈ 160 °C, in agreement with the *in situ* SPXRD.

A number of control reactions were executed to support the proposal that it is indeed the exposure to atmospheric H_2O that promotes the amorphous intermediate formation. If the reactants are instead sealed with ca. 1/3 atm of O_2, no color change is observed after 1 h at room temperature. Alternatively, a pellet of the reactants in ambient air turns black within seconds. If the reaction mixtures sealed with O_2 are then heated to 100 °C for 1 h, PXRD analysis of the mixtures indicates that only the reactants MCl_2 and Na_2S_2 are still present, which is identical to the air-free reactions (Figure S7).

DISCUSSION

Taken together, these results illustrate that the presented kinetically controlled solid-state metathesis reactions have been executed in a manner that circumvents diffusion to produce crystalline material in the bulk. Thin-film metallurgical junctions have been shown to exhibit kinetically controlled reactions that are not diffusion limited.[30,31] As the film thickness increases, one tends to observe a range of intermediate compounds due to the limited diffusion of reactants through the film.[32] By limiting the thickness of the thin films, a distinct solid-state reaction mechanism in which the reactants completely interdiffuse before nucleation of a crystalline phase is observed, as initially shown with iron silicides[30] among other examples.[33] When crystalline, kinetic intermediates are observed, the first phase to form is not necessarily the most thermodynamically stable,[34] but rather, it has been proposed that the first phase to form is that which allows the largest change in free energy in the shortest period of time (i.e., greatest $\Delta G/\Delta t$).[35,36] This rationalizes the observation of metastable Fe_5Si_3 (a high-temperature phase) in binary Fe−Si couples at low temperature, as well as the formation of amorphous phases.[34] However, it has not been clear how to achieve kinetic control in the synthesis of materials without an intentionally reduced diffusion length.

DOI: 10.1021/jacs.6b06367
J. Am. Chem. Soc. 2016, 138, 11031−11037

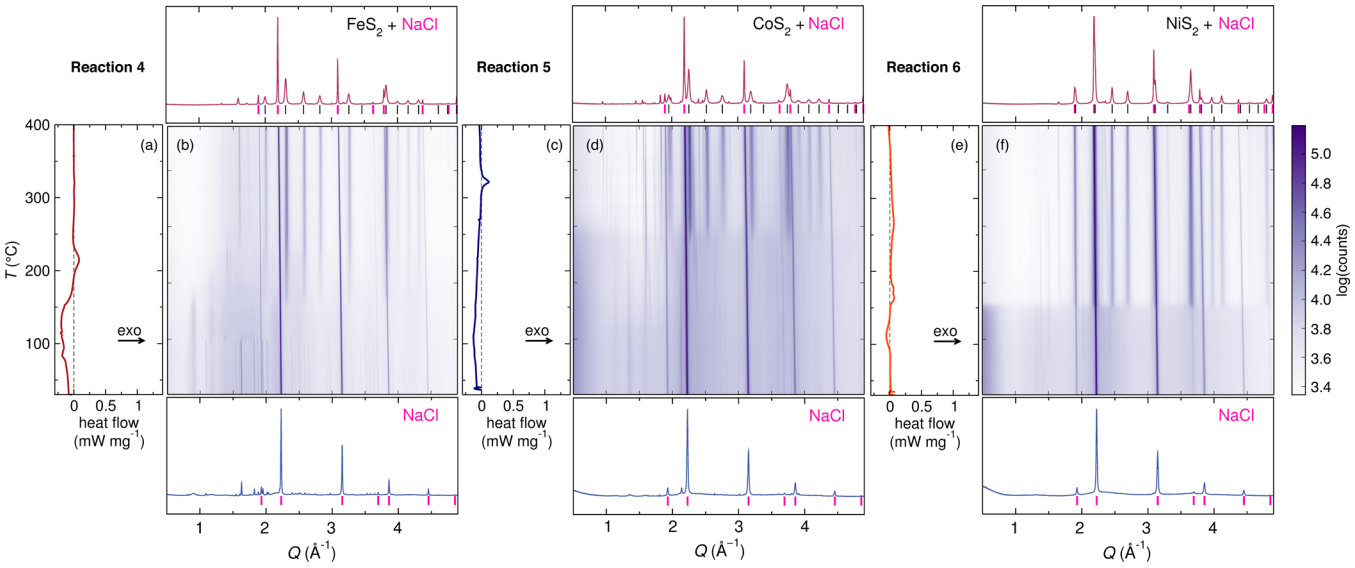

Figure 3. *In situ* DSC (a, c, e) and SXRD (b, d, f) of the air-exposed solid-state metathesis reactions of $MCl_2 + Na_2S_2 \rightarrow MS_2 + 2$ NaCl, M = Fe (reaction **4**), Co (reaction **5**), and Ni (reaction **6**), respectively. In the air-exposed reactions, the reaction pathway is extensively altered compared to the air-free reactions, with NaCl present throughout and no apparent crystalline intermediates, and the products instead crystallizing out of the reaction mixtures. There are significant diffuse features in the background as well, indicating the presence of an amorphous phase. This is especially apparent in **5** and **6**. The diffraction patterns of the as-prepared reactants and the products at 400 °C are shown below and above each color plot, respectively.

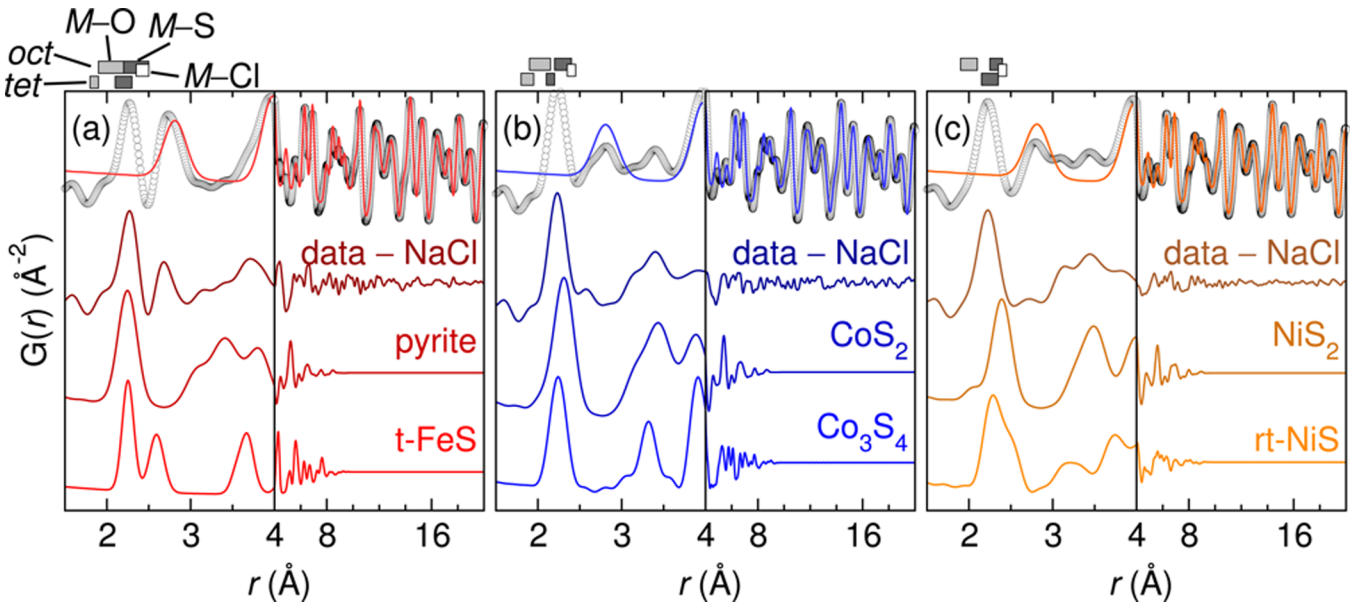

Figure 4. Pair distribution function (PDF) analyses of the as-prepared air-exposed reaction mixtures for (a) reaction **4**, (b) reaction **5**, and (c) reaction **6**. Fits to NaCl were applied, and the difference (data − NaCl) was then compared to calculated PDFs of a number of transition metal sulfides (bottom two lines). The calculated PDFs are truncated using a spherical diameter particle cutoff of 10 Å. Qualitative comparison to the difference curves indicates that all reaction mixtures have some structural similarities to the MS_2 product that forms.

The metathesis reactions prepared in an inert argon environment are diffusion limited, akin to "thick" film diffusion couple reactions. This conclusion is based upon the observation of a range of sulfur-poor intermediates in all cases, which are both stable (e.g., Fe_7S_8, Co_3S_4, rt-NiS) and metastable (e.g., Fe_3S_4, CoS, ht-NiS) with respect to the reaction conditions at the time of their observation. This indicates that the reaction is essentially progressing as metal and sulfide ions crystallizing as they interdiffuse after NaCl has formed, forming a range of MS_x intermediates before reaching the stoichiometric MS_2 product, depending on the degree of diffusion that has occurred at a given temperature. This sampling of the phase diagram agrees with fundamental studies of diffusion couples in solids and strongly indicates that the reaction is indeed diffusion limited.[34,35] It is possible that amorphous MS_x intermediates may also form, but their presence is not immediately evident from the *in situ* diffraction experiments. Here, the onset of reactivity, indicated by the formation temperature of NaCl (Figure 2), correlates with the enthalpy of formation of the metal chloride precursor (Figure S5). The enthalpy of formation of the metal sulfide products shows no such correlation. Our observations are also consistent with the

DOI: 10.1021/jacs.6b06367
J. Am. Chem. Soc. 2016, 138, 11031−11037

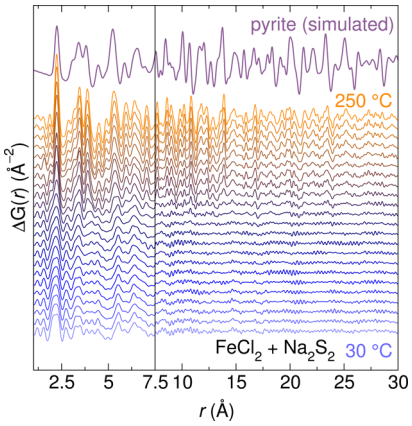

Figure 5. *In situ* differential PDF analysis of reaction **4** ($FeCl_2$ + Na_2S_2) with the pairwise correlations arising from NaCl subtracted. The differential PDF at lower temperatures reveals only short-range correlations; longer-range correlations consistent with crystallization gradually grow in starting around $T \approx 160$ °C, in agreement with *in situ* PXRD data. The high-temperature differential PDF is identical to that of pyrite FeS_2. The offset data are taken in 10 °C increments.

contrasting self-igniting metathesis reactions, in which one observes an initial "induction period".[15,17−21] There, the initial formation of NaCl at lower temperatures causes displacement of the metal and sulfur counterions. The diffusion-limited process then initiates the exothermic reaction that self-heats the reaction mixture enough to melt the alkali halide, thus allowing for rapid diffusion of the reagents.

If the solid-state metathesis reactions are first ground in ambient atmosphere before sealing under vacuum and annealing (reactions **4**−**6**), NaCl forms, and a color change to black occurs in all cases. Annealing these reaction mixtures yields direct formation of the MS_2 product at lower temperatures than those needed for the air-free reactions, and with much less heat released (see Table 1). In contrast to the air-free, diffusion-limited reactions, these partially hydrated reactions show no crystalline intermediates before MS_2 product formation. Grinding in air clearly alters the energetic and structural pathways to product formation, yielding an amorphous intermediate that releases little energy upon crystallization. Additionally, we have previously shown that this air exposure does not negatively affect the properties of the resultant material, exemplified by the superconducting transition of metastable cubic $CuSe_2$.[25]

The formation of the amorphous precursor is a significant alteration to the reaction mechanism. This, in conjunction with the observation of direct MS_2 crystallization, suggests that the air-exposed reactions are limited by nucleation of the product phase rather than diffusion of the reactants. Regardless of the transition metal, the nearest neighbor in the as-ground PDF corresponds to M−S bond lengths for a low coordination number, rather than metal−oxygen or metal−halogen bonds (Figure 4). Here, we speculate that the formation of an amorphous intermediate that has the lowest stable coordination geometry of the transition metal with sulfur provides the maximum $\Delta G/\Delta t$ in a kinetically controlled reaction. In all of these cases we observe an intermediate amorphous phase that resembles the most dense, and lowest coordination number, known for these transition metal sulfides (tet-FeS, Co_3S_4, NiS).

The formation of the M−S bonds upon grinding the reactants in air aids in explaining why the annealing is so much less exothermic than in the air-free reactions. Rather than breaking and making bonds, the intermediate undergoes subtle rearrangements and crystallization, akin to the nucleation of metastable $FeSb_3$ from modulated elemental reactants in a thin-film geometry.[37] Analysis of the *in situ* diffraction profile at the approximate onset of MS_2 crystallization indicates that the MS_2 phases form initially as small nanosized crystallites (ca. hundreds of angstroms) that grow upon annealing, which will have a distinct thermodynamic signature spread out over a wide range of temperatures, as opposed to a sharp crystallization transition.

The key to altering the reaction pathway of these reactions from diffusion-limited to nucleation-limited is grinding the reactants in air. We previously showed that the air exposure of a metathesis reaction can lead to the formation of a metastable cubic polymorph of $CuSe_2$.[25] We later confirmed that a trace amount of a Lewis base, such as triphenylphosphine, mirrors this chemical activity by facilitating atom-transfer reactions during the double exchange reaction, as noted by the observation of stable adducts (e.g., $Se{:}PPh_3$, $[Cu(PPh_3)_n]^+$).[26] In thin-film diffusion couples (i.e., modulated elemental reactions[30,31,33,37]), solid-state interdiffusion is achieved at lower temperature by decreasing the physical length scale over which the reagents must diffuse to form the new material. As summarized in Figure 6, we show that a chemical additive, such as trace $H_2O(g)$, can accomplish the same effect in a solid-state metathesis reaction to circumvent solid-state diffusion.

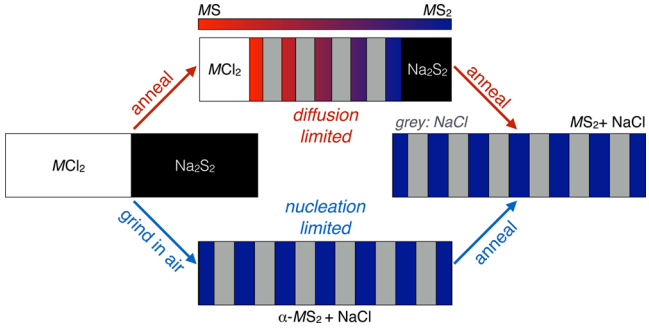

Figure 6. Scheme illustrating the different observed reaction pathways of the metathesis reactions. Preparing the reactants in a strictly air-free and anhydrous manner leads to a diffusion-limited reaction which in turn allows the formation of a range of MS_x phases ($x \leq 2$). Grinding the reactants in air allows NaCl formation along with an amorphous (α) material of the nominal composition MS_2. Annealing leads to direct nucleation of the crystalline MS_2 phase.

CONCLUSIONS

The solid-state metathesis reactions of MCl_2 + Na_2S_2 show the structural signatures from the progression of reactants to intermediates to products, determined from *in situ* structural and thermochemical analysis of the reactions. However, the formation of NaCl in anhydrous metathesis reactions proceeds slowly and without appreciable energy release. The gradual formation of NaCl allows displacement of the M and S counterions to form intermediates that are substoichiometric with respect to the final products, such as metal−sulfide binaries, a range of Na_2S_x phases, and some ternary phases. If the reactants are exposed to humid air, H_2O can facilitate atom transfer before heating; thus, crystalline NaCl forms directly along with an amorphous M−S phase with a low coordination

DOI: 10.1021/jacs.6b06367
J. Am. Chem. Soc. 2016, 138, 11031−11037

number. This indicates that the reaction is no longer limited by solid-state diffusion (i.e., the NaCl and M−S bonds have already formed). Instead, product formation is limited by nucleation of the crystalline MS_2 phase. The results provide the pathway to direct synthetic solid-state chemistry toward a paradigm of materials by design. From these results, one can design a wide range of reactions to target discovery of new metastable polymorphs or stable compounds that have not been kinetically accessible using traditional solid-state chemistry.

MATERIALS AND METHODS

All reactants were prepared and stored an argon-filled glovebox with H_2O and O_2 levels ≤0.1 ppm. All transition metal chlorides were used as purchased, with purity >98%. Na_2S_2 was synthesized through the indirect reaction of Na + S; in a sealed 14 mm i.d. vitreous silica tube, an alumina crucible containing purified elemental sulfur was placed on top of an alumina crucible containing ≈1.02 equiv of elemental sodium. The excess was to account for observable oxidation on the surface of the sodium metal. The reactants were then heated at 200 °C for 24 h, at which point all material could be found in the originally sodium containing crucible. The heterogeneous product was then collected in the glovebox, ground, pelleted, and resealed, and then heated at 300 °C for 24 h to form Na_2S_2, at which point a yellow powder was collected in the glovebox. To confirm purity of the Na_2S_2, air-free powder diffraction data were collected in a sealed glass capillary using a Bruker APEX II single crystal diffractometer (Mo Kα radiation, λ = 0.7107 Å). Laboratory PXRD data were collected with Bruker D8 Discover X-ray diffractometer using a Cu Kα radiation and a Lynxeye XE-T position-sensitive detector. Air-sensitive samples were prepared on a zero-diffraction off-axis Si wafer in an argon glovebox before being sealed off with Kapton tape.

The reaction mixtures of MCl_2 and Na_2S_2 were combined in 1:1 stoichiometric ratios and ground homogeneously. They were then evacuated and sealed in extruded silica capillaries (o.d. = 0.7 mm). For air-exposed reactions, the reaction mixtures were ground homogeneously in an Ar-filled glovebox, and then removed to a fume hood in ambient atmosphere. The reaction mixtures all begin to darken in appearance within seconds and are completely black after ca. 60 s of grinding. Exact humidity levels were not controlled, but were generally ≤50% as monitored by an ambient humidity sensor. The reactant mixtures do not deliquesce. The reaction mixtures were then evacuated to <10 mTorr and sealed in extruded silica capillaries. *In situ* synchrotron X-ray diffraction data was collected using beamline 17-BM-B (λ = 0.75009 Å) at the Advanced Photon Source at Argonne National Laboratory. The samples were heated at 3 °C min^{-1} from room temperature to 400 °C using a resistive heater as previously described.[38] Diffraction data were continuously collected using a 2048 × 2048 pixel PerkinElmer 2D plate detector in 30 s increments, each pattern consisting of three 10 s subframes, while the sample was continuously rotated by 5° along its long axis. The 2D diffraction patterns were then radially integrated using GSAS-II.[39] A LaB_6 standard (NIST 660b) was used to calibrate the sample-to-detector distance, which was nominally 300 mm. *Ex situ* total scattering data were collected on beamline 11-ID-B (λ = 0.2114 Å) at the Advanced Photon Source at Argonne National Laboratory. The *in situ* total scattering data were collected on beamline 11-ID-C (λ = 0.1115 Å) at 10 °C intervals, and the data was then radially integrated using Fit2D.[40] The pair distribution functions $G(r)$ were then extracted using PDFgetX3[41] and fit using PDFGUI.[42] Rietveld analyses were performed using EXPGUI/GSAS.[43,44] Sequential Rietveld refinements were executed in small sections (determined by visual inspection), and maximum damping was applied to prevent unphysical outcomes in the fits.

Differential scanning calorimetry data were collected on a TA Instruments DSC on homogeneously ground reaction mixtures (approximately 10 mg) hermetically sealed in aluminum cans. The temperature ramp was 3 °C min^{-1} to replicate the reaction collected *in situ*. The enthalpy of each reaction was approximated by integrating the DSC curves after subtracting a linear baseline. Hess's law calculations were performed using tabulated values for the standard formation energy of the reactants and products.[45]

ASSOCIATED CONTENT

Supporting Information

The Supporting Information is available free of charge on the ACS Publications website at DOI: 10.1021/jacs.6b06367.

Additional discussion of *in situ* powder X-ray diffraction data, selected Rietveld refinements of *in situ* powder X-ray diffraction data, experimentally observed formation temperatures of products compared to heats of formation, *in situ* X-ray pair distribution function analysis data of reaction **1**, and PXRD data of O_2 gas-exposed control reactions (PDF)

AUTHOR INFORMATION

Corresponding Author

*james.neilson@colostate.edu

Notes

The authors declare no competing financial interest.

ACKNOWLEDGMENTS

A.J.M. and J.R.N. acknowledge financial support from the W. M. Keck Foundation. This research used resources of the Advanced Photon Source, a U.S. Department of Energy (DOE) Office of Science User Facility operated for the DOE Office of Science by Argonne National Laboratory under contract no. DE-AC02-06CH11357. The authors gratefully acknowledge Dr. G. Halder for his assistance collecting *in situ* powder X-ray diffraction data at beamline 17-BM-B, and Dr. O. Borkiewicz for his assistance collecting total X-ray scattering data at beamlines 11-ID-B and 11-ID-C.

REFERENCES

(1) DiSalvo, F. J. *Science* **1990**, *247*, 649−655.
(2) Stein, A.; Keller, S. W.; Mallouk, T. E. *Science* **1993**, *259*, 1558−1564.
(3) Kanatzidis, M. G.; Poeppelmeier, K. R.; et al. *Prog. Solid State Chem.* **2008**, *36*, 1−133.
(4) Buck, M. R.; Bondi, J. F.; Schaak, R. E. *Nat. Chem.* **2012**, *4*, 37−44.
(5) Gopalakrishnan, J. *Chem. Mater.* **1995**, *7*, 1265−1275.
(6) Murphy, D. W.; Cros, C.; DiSalvo, F. J.; Waszczak, J. V. *Inorg. Chem.* **1977**, *16*, 3027−3031.
(7) Neilson, J. R.; McQueen, T. M. *J. Am. Chem. Soc.* **2012**, *134*, 7750−7757.
(8) Kobayashi, Y.; Hernandez, O.; Sakaguchi, T.; Yajima, T.; Roisnel, T.; Tsujimoto, Y.; Morita, M.; Noda, Y.; Mogami, Y.; Kitada, A.; Ohkura, M.; Hosokawa, S.; Li, Z.; Hayashi, K.; Kusano, Y.; Kim, J. e.; Tsuji, N.; Fujiwara, A.; Matsushita, Y.; Yoshimura, K.; Takegoshi, K.; Inoue, M.; Takano, M.; Kageyama, H. *Nat. Mater.* **2012**, *11*, 507−511.
(9) Yajima, T.; Takeiri, F.; Aidzu, K.; Akamatsu, H.; Fujita, K.; Yoshimune, W.; Ohkura, M.; Lei, S.; Gopalan, V.; Tanaka, K.; Brown, C. M.; Green, M. A.; Yamamoto, T.; Kobayashi, Y.; Kageyama, H. *Nat. Chem.* **2015**, *7*, 1017−1023.
(10) Mikita, R.; Aharen, T.; Yamamoto, T.; Takeiri, F.; Ya, T.; Yoshimune, W.; Fujita, K.; Yoshida, S.; Tanaka, K.; Batuk, D.; Abakumov, A. M.; Brown, C. M.; Kobayashi, Y.; Kageyama, H. *J. Am. Chem. Soc.* **2016**, *138*, 3211−3217.
(11) Kanatzidis, M. G. *Chem. Mater.* **1990**, *2*, 353−363.
(12) Shoemaker, D. P.; Chung, D. Y.; Mitchell, J. F.; Bray, T. H.; Soderholm, L.; Chupas, P. J.; Kanatzidis, M. G. *J. Am. Chem. Soc.* **2012**, *134*, 9456−9463.

DOI: 10.1021/jacs.6b06367
J. Am. Chem. Soc. 2016, 138, 11031−11037

(13) Shoemaker, D. P.; Hu, Y.-J.; Chung, D. Y.; Halder, G. J.; Chupas, P. J.; Soderholm, L.; Mitchell, J. F.; Kanatzidis, M. G. *Proc. Natl. Acad. Sci. U. S. A.* **2014**, *111*, 10922−10927.
(14) Bonneau, P. R.; Shibao, R. K.; Kaner, R. B. *Inorg. Chem.* **1990**, *29*, 2511−2514.
(15) Bonneau, P. R.; Jarvis, R. F.; Kaner, R. B. *Nature* **1991**, *349*, 510−512.
(16) Bonneau, P. R.; Jarvis, R. F.; Kaner, R. B. *Inorg. Chem.* **1992**, *31*, 2127−2132.
(17) Wiley, J.; Kaner, R. *Science* **1992**, *255*, 1093−1097.
(18) Gillan, E. G.; Kaner, R. B. *Chem. Mater.* **1996**, *8*, 333−343.
(19) Parkin, I. P. *Chem. Soc. Rev.* **1996**, *25*, 199−207.
(20) Shaw, G. A.; Morrison, D. E.; Parkin, I. P. *J. Chem. Soc., Dalton Trans.* **2001**, 1872−1875.
(21) Nartowski, A. M.; Parkin, I. P.; Craven, A. J.; MacKenzie, M. *Adv. Mater.* **1998**, *10*, 805−808.
(22) Cumberland, R. W.; Weinberger, M. B.; Gilman, J. J.; Clark, S. M.; Tolbert, S. H.; Kaner, R. B. *J. Am. Chem. Soc.* **2005**, *127*, 7264−7265.
(23) Chung, H.-Y.; Weinberger, M. B.; Levine, J. B.; Kavner, A.; Yang, J.-M.; Tolbert, S. H.; Kaner, R. B. *Science* **2007**, *316*, 436−439.
(24) Martinolich, A. J.; Neilson, J. R. *J. Am. Chem. Soc.* **2014**, *136*, 15654−15659.
(25) Martinolich, A. J.; Kurzman, J. A.; Neilson, J. R. *J. Am. Chem. Soc.* **2015**, *137*, 3827−3833.
(26) Martinolich, A. J.; Higgins, R. F.; Shores, M. P.; Neilson, J. R. *Chem. Mater.* **2016**, *28*, 1854−1860.
(27) Waldner, P.; Pelton, A. *J. Phase Equilib. Diffus.* **2005**, *26*, 23−38.
(28) Kuznetsov, V.; Sokolova, M.; Palkina, K.; Popova, Z. *Inorg. Mater.* **1965**, *1*, 617−632.
(29) Waldner, P.; Pelton, A. D. *Z. Metallkd.* **2004**, *95*, 672−681.
(30) Novet, T.; Johnson, D. C. *J. Am. Chem. Soc.* **1991**, *113*, 3398−3403.
(31) Fister, L.; Johnson, D. C. *J. Am. Chem. Soc.* **1992**, *114*, 4639−4644.
(32) Gösele, U.; Tu, K. *J. Appl. Phys.* **1989**, *66*, 2619−2626.
(33) Johnson, D. C. *Curr. Opin. Solid State Mater. Sci.* **1998**, *3*, 159−167.
(34) Walser, R.; Bené, R. *Appl. Phys. Lett.* **1976**, *28*, 624−625.
(35) Gösele, U.; Tu, K. *J. Appl. Phys.* **1982**, *53*, 3252−3260.
(36) Bené, R. *J. Appl. Phys.* **1987**, *61*, 1826−1833.
(37) Bauers, S. R.; Wood, S. R.; Jensen, K. M.; Blichfeld, A. B.; Iversen, B. B.; Billinge, S. J.; Johnson, D. C. *J. Am. Chem. Soc.* **2015**, *137*, 9652−9658.
(38) Chupas, P. J.; Chapman, K. W.; Kurtz, C.; Hanson, J. C.; Lee, P. L.; Grey, C. P. *J. Appl. Crystallogr.* **2008**, *41*, 822−824.
(39) Toby, B. H.; Von Dreele, R. B. *J. Appl. Crystallogr.* **2013**, *46*, 544−549.
(40) Hammersley, A. P.; Svensson, S. O.; Hanfland, M.; Fitch, A. N.; Hausermann, D. *High Pressure Res.* **1996**, *14*, 235−248.
(41) Juhás, P.; Davis, T.; Farrow, C. L.; Billinge, S. J. L. *J. Appl. Crystallogr.* **2013**, *46*, 560−566.
(42) Farrow, C. L.; Juhas, P.; Liu, J. W.; Bryndin, D.; Božin, E. S.; Bloch, J.; Proffen, T.; Billinge, S. J. L. *J. Phys.: Condens. Matter* **2007**, *19*, 335219.
(43) Toby, B. H. *J. Appl. Crystallogr.* **2001**, *34*, 210−213.
(44) Larson, A.; Von Dreele, R. *General Structure Analysis System (GSAS)* Los Alamos National Lab, 2004.
(45) Lide, D. R. *CRC Handbook of Chemistry and Physics*, 87th ed.; CRC Press, 2005.

DOI: 10.1021/jacs.6b06367
J. Am. Chem. Soc. 2016, 138, 11031−11037